Spin scan tomographic array-based imager

Harald Hovland

Norwegian Defence Research Establishment (FFI), Postboks 25, NO-2027 Kjeller, Norway
*harald.hovland@ffi.no

Abstract: This work presents a novel imaging device based on tomographic reconstruction. Similar in certain aspects to the earlier presented tomographic scanning (TOSCA) principle, it provides several important enhancements. The device described generates a stream of one-dimensional projections from a linear array of thin stripe detectors onto which the (circular) image of the scene is rotated. A two-dimensional image is then reproduced from the one-dimensional signals using tomographic processing techniques. A demonstrator is presented. Various aspects of the design and construction are discussed, and resulting images and movies are presented.

OCIS codes: (070.0070) Fourier optics and signal processing; (100.6950) Tomographic image processing; (110.0110) Imaging systems; (110.3010) Image reconstruction techniques; (110.6960) Tomography.

References and links

1. H. Hovland, "Tomographic scanning imager," Opt. Express **17**(14), 11371–11387 (2009).
2. H. Hovland, "Construction and demonstration of a multispectral tomographic scanning imager (TOSCA)," Opt. Express **21**(4), 4688–4702 (2013).
3. H. Hovland, "Experimental tomographic scanning (TOSCA) imagers," Proc. SPIE **9070**, 90700H (2014).
4. A. C. Kak and M. Slaney, *Principles of Computerized Tomographic Imaging* (IEEE, 1988). *http://www.slaney.org/pct/pct-toc.html*.
5. R. N. Bracewell and A. C. Riddle, "Inversion of fan-beam scans in radio astronomy," Astrophys. J. **150**, 427–434 (1967).
6. G. T. Herman, *Image Reconstructions from Projections* (Academic, 1980).
7. A. H. Andersen and A. C. Kak, "Simultaneous algebraic reconstruction technique (SART): A superior implementation of the art algorithm," Ultrason. Imaging **6**(1), 81–94 (1984).
8. H. Hovland, "Specialized tomographic scanning imaging seeker," Proc. SPIE **5778**, 725–731 (2005).

1. Introduction

Tomographic scanning (TOSCA) imaging was presented earlier [1] as an alternative way of acquiring images using various types of radiation. In the TOSCA imager, thin lines scan the scene at regular angular intervals, as seen in Fig. 1(a). These 1-dimensional scans are then processed with tomographic reconstruction techniques to reproduce a 2-dimensional image.

In [1], it was shown that a single pixel sensor combined with a simple circular conical scan mechanism could produce images with better signal-to-noise ratio than achievable with classical single pixel imagers using 2D scanning, and demonstrators were presented in [2, 3] as proofs-of-concept. The working principle used in the demonstrators is shown in Figs. 1(b) and 1(c). It was shown that the concept could give adequate image quality for a low-noise silicon detector with reasonable light conditions, but the typical noise levels of detectors operating in the infrared domain restricts the useful imaging to very hot objects, very limited resolution or imaging of static objects with relatively long exposure times.

An array-based TOSCA imager concept was also proposed in [1], potentially producing images with better signal-to-noise ratio than that of a classical broom-scan linear array. The circular array would then be similar to the reticle shape in Fig. 1(c), but because several line detectors can be in the field of view (FOV) simultaneously, the detector spacing could be so small that the detectors touch each other, reducing the scan circle and simplifying the optics.

#224954 - $15.00 USD Received 15 Oct 2014; revised 24 Nov 2014; accepted 29 Nov 2014; published 18 Dec 2014

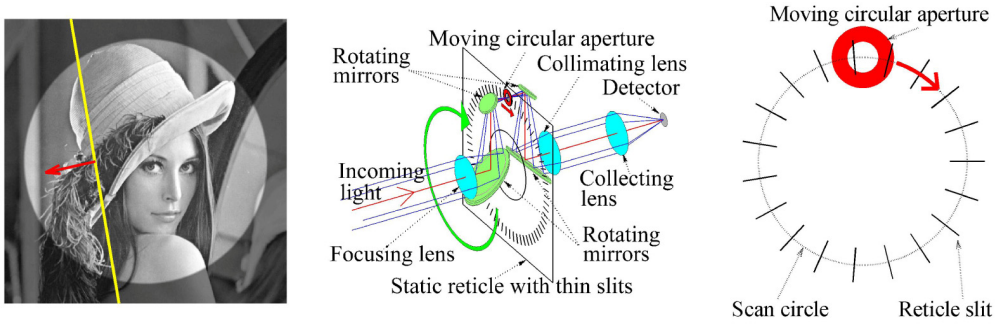

Fig. 1. (a) TOSCA imaging: A thin line detector (yellow line) scans across the image of the scene, the latter being restricted by an aperture. Alternatively, an array can replace the single line detector. The scan is repeated at different angles. (b) Conical scan TOSCA working principle used in the demonstrator presented in [2, 3]. The mirrors (green) and the aperture (red) rotate as a unit around the optical axis of the incoming light. The image orientation remains fixed relative to the reticle, therefore the thin slits scan the image at regular angular intervals. (c) Reticle pattern and moving aperture layout. The aperture (in red), defining the field of view, moves in a circle. The use of an aperture enables the use of a single detector element to make all the angular scans without aliasing as only one slit transmits light from the scene to the detector at any time. All images are reproduced from [2].

This paper presents a new array-based tomographic scanning imager design making use of spin scan optics. The spin scan TOSCA imager has a potentially better noise performance than a conventional line scan imager, and with the right readout electronics it has a capability for detection and, to a certain degree, also characterization and localization of transients that can be faster than the time constants associated with the frame rate. It is therefore suitable for use in low cost sensor in unmanned aerial vehicles, especially systems looking for or at fast phenomenons.

The new design represents a clear improvement to the previously presented conical scan TOSCA design, both in terms of performance and manufacturability. Several implementations are proposed for the optics of such a system.

An experimental demonstrator based on this design is presented, operating in the mid-infrared range. The aim of this demonstrator is to show a practical implementation of this TOSCA imager concept, also illustrating artifacts that can arise. The camera design is presented, including the signal processing necessary for the image reconstruction. Sources of noise and systematic errors are discussed. Simulations highlight important design considerations.

2. Spin scan TOSCA design

2.1 Basic principle

The basic spin scan TOSCA sensor principle is illustrated in Fig. 2. It consists of optics that focuses an image of the scene onto a linear detector array, while rotating the scene image relative to the linear array.

The detector array FOV could be limited either by a circular aperture in front of it, or by adapting the active length of each detector to a corresponding circle. Thus the number of spatial samples across the FOV for one angular scan is given by the physical linear array, but the number of angular scans is given by the sample rate and the optics rotational speed. This is the opposite of the conical scan TOSCA, where the rotational speed defines the number of samples per angular scan, whereas the array or reticle determines the number of angular scans.

#224954 - $15.00 USD Received 15 Oct 2014; revised 24 Nov 2014; accepted 29 Nov 2014; published 18 Dec 2014

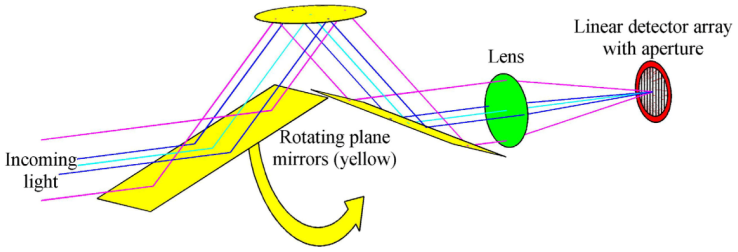

Fig. 2. Spin scan TOSCA imaging: A rotating image of the scene is projected onto a linear detector array. This example features the use of three rotating plane mirrors and a lens. The mirrors (yellow) that flip the image of the scene rotate as a unit with respect to the scene, while the detector array remains stationary.

Once the signal has been sampled, the reconfiguration follows classical parallel beam tomography reconstruction [4]. A short description of the procedure used here is as follows:

1. The signals are sampled for *M* regularly distributed angular positions around the circle for each TOSCA reconstruction.
2. *N* samples are made per angular position, one for each of the *N* detectors.
3. Zero pad the *N* samples to limit the fast Fourier transform (FFT) continuous boundary effects, adding at least *N* extra samples. Letting the number Z of zero-padded samples be a power of two optimizes the subsequent processing.
4. Take the FFT of each zero-padded sample series.
5. Multiply the components of the resulting FFT series value by value with its corresponding absolute frequency value, with the exception of the first (zero frequency) coefficient, which should be ¼: {¼, 1, 2, …, Z/2, Z/2-1, … 2, 1}. If needed, modify this ramp filter with an application-specific smoothing filter.
6. Take the inverse FFT of the product. Remove excess samples added in point 3.
7. For each angular position, produce a back projection matrix where each pixel is given the (linearly) interpolated value of the series found in point 6, the indices being based on the pixel's orthogonal projected position on the scan line. The back projection matrix resolution can be different from that of the initial scan.
8. The reconstruction is completed by summing up all the filtered back projection matrices (and normalizing if needed).

The filtered back projection technique, originally developed by Bracewell et al [5], has been found to be an efficient first order method. It is possible to improve the result by (iterative) algebraic reconstruction techniques [6, 7]. This, however, might not be acceptable in a real-time system due to unwanted latency or high computational requirements.

2.2 Optical configurations

The spinning scan optics can be realized in several alternative ways, as shown in Fig. 3. In the simplest form, the focusing optics and the linear detector array are rotating together as in Fig. 3(a), a concept useful in for example rotating projectiles.

A combination of rotating optics with an odd number of reflecting surfaces such as the depicted dove prism in Fig. 3(b), or the three reflecting mirrors shown in Fig. 2, provides the flipping of the field of view and rotation, while regular focussing optics provides the imaging.

A particularly compact solution is seen in Fig. 3(c), where a toroidal concave primary mirror opposes a cylindrical (or toroidal) concave secondary mirror, both rotating as a unit. This configuration, not seen before in the literature by the author, enables a compact

#224954 - $15.00 USD Received 15 Oct 2014; revised 24 Nov 2014; accepted 29 Nov 2014; published 18 Dec 2014

combined focussing and flipping of the image using only two optical elements. An equivalent, but less compact solution based on regular and cylindrical lenses is shown in Fig. 3(d).

If only the optics is rotating, the FOV angular speed will be twice that of the optics. In [1, 2, 8], a point was made in having an odd number of angular scans, as two angular scans with a 180° shift contain equivalent information. For the spin scan configuration, the situation is the same for a symmetrically mounted linear array, and scans during a ½ FOV rotation relative to the linear array enable a complete image reconstruction. If, however, the linear array is shifted by ¼ pixels sideways, a doubling of the sampling density can be achieved with a 32 element linear array sampling 64 pixels across the FOV based on two angular scans separated by 180°. A complete scan then requires a 360° scene image rotation relative to the linear array. This doubling in spatial resolution should also be followed by an additional doubling of the number of angular steps, quadrupling the number of angular scan positions.

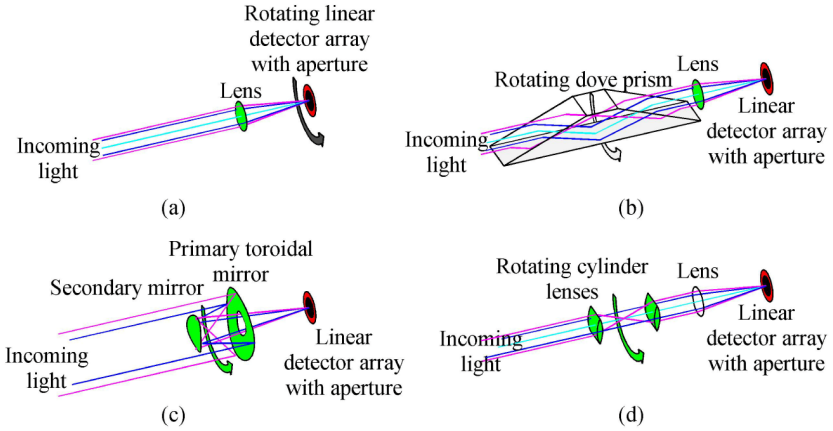

Fig. 3. Alternative TOSCA spin scan optical configurations: (a) Rotating detector array. (b) An odd number of reflecting, rotating planes, for example a dove prism (or three reflective mirrors as in Fig. 2). (c) A toroidal primary mirror facing a secondary toroidal or cylindrical mirror. A similar effect can be obtained using thick refractive optics, with one toroidal front surface and one toroidal or cylindrical back surface. (d) A similar realisation using a combination of two cylindrical lenses and one spherical lens.

3 Comparison of the spin scan versus the conical scan TOSCA configurations

3.1 Photon efficiency

In the reticle based (single pixel) conical scan TOSCA configuration, only one scan line can be in the FOV at the same time. This limits the FOV covered by the detector active area at any given time. Define, as before [1], the photon harvesting efficiency as the average proportion of the incoming photons collected by the sensor. Assuming an idealized sensor and optics where the aperture diameter is N times the slit width, the maximum photon harvesting efficiency for the reticle based configuration is N^{-1}. This can be seen by noting that the slot in the reticle covers the equivalent of one of the N pixel rows at any time.

If the reticle is replaced by M individual line detectors arranged in a radial pattern, several detectors can be in the field of view at the same time. This allows a reduced scan circle diameter, and also increases the photon harvesting efficiency compared to the reticle based configuration. M then represents the number of scan angles. We assume in the following that the aperture diameter is N times the detector width. This means N represents a measure of the number of pixels both along and across the scan direction.

The theoretical upper limit of the photon harvesting efficiency is found by geometric considerations to be $M/(M + \pi N)$: In this optimum conical scan array-based configuration, the

#224954 - $15.00 USD Received 15 Oct 2014; revised 24 Nov 2014; accepted 29 Nov 2014; published 18 Dec 2014

M radially oriented detectors are arranged in a star-shaped circular array, such that one end of each of the M radially oriented detectors touches those of its two neighbours, forming a closed inner circle from which the detectors extend, with a diameter of M/π times the detector width. If the scan circle crosses the middle of each line detector, the scan circle diameter is $M/\pi + N$ detector widths, giving a scan line perimeter of $M + \pi N$ detector widths. Assuming one sample is made per detector width along the scan circle, and noting that each pixel is scanned one time by each of the M detector lines per frame, the photon harvesting efficiency becomes approximately $M/(M + \pi N)$. This is an approximation, as the scan velocity vector is generally not exactly normal to the line detector orientation.

The expression $M/(M + \pi N)$ degenerates to the value $(1 + \pi)^{-1} \approx ¼$ reported in [1] in the case where $N = M$. The value of this expression could in principle approach unity if the number of scan angles (and hence detectors) is much larger than the aperture to slit width ratio N. For practical configurations, however, the photon harvesting efficiency is likely to be below ½ for the array based conical scan TOSCA configuration. In contrast, the parallel structure of the line detector array in the spin scan TOSCA configuration presented here allows practically the whole scene to be projected onto active detector surfaces at any time, giving an idealized system a unity photon harvesting efficiency. This would be on par with a 2D focal plane array.

As was described in [8], the conical scan TOSCA configuration was demonstrated to be able to handle modulation levels higher than the frame rate. The reason for this capability is that the total FOV is scanned many times per frame, so that an assessment of the total signal level could be made and compensated for. The spin scan TOSCA has a similar, but better assessment capability, due to both the potential near unit photon harvesting efficiency and simultaneous 1-dimensional localization possibility of strong transients. The detection of fast transients could be done by monitoring the total energy of the FOV for one angular position, and the localisation could be made by comparing the energy in individual detectors from neighbouring angular positions or previous frames. The same comparison could also be used to compensate for undesirable transients.

3.2 Signal to noise performance

The detector bandwidth required to adhere to the Nyquist criterion is $2 \times f \times$ <*samples/frame*>. For the TOSCA spin scan array configuration here would be $2 \times f \times M$, where f is the image frame rate and M the number of angular scan positions per frame. In comparison, the TOSCA conical scan array configuration detector bandwidth required would be slightly higher, $2 \times f \times (M + \pi N)$, as higher scan speed is required to scan across the more sparsely distributed detectors, the number of scans being developed above. In line with the analysis in [1], the signal to noise level would be around $(1 + \pi) \approx 4$ times better in a spin scan TOSCA configuration than in a corresponding optimized conical scan array based TOSCA configuration, and with a signal-to-noise ratio $M^{-½}$ relative to that of an idealized 2D detector array, based on the pure detector bandwidth requirement.

A more detailed noise analysis can be made by considering the TOSCA model with the following assumptions: The scene is uniformly illuminated, and the detectors are shot noise limited with Poisson noise statistics, with negligible noise in the readout electronics. We can define (virtual) pixels in the scene image on the detector array, each pixel being square with the side equal to the width of each line detector.

The inverse fast Fourier transform (IFFT) of the ramp filter (which is in the Fourier domain) used to create the filtered back projection of each scan represents the coefficient with which each pixel will contribute to the final central pixel for a given angular scan. As was also found in [1] for the conical scan TOSCA configuration, the central pixel will get the highest noise contribution from the other pixels in a scene, and therefore represents a conservative noise estimate for the system. Assuming a uniformly illuminated scene that does not change during one frame, a well reproduced filter with a sufficiently high number of

#224954 - $15.00 USD Received 15 Oct 2014; revised 24 Nov 2014; accepted 29 Nov 2014; published 18 Dec 2014

angular scan positions and detectors per scan will ideally create orthogonality, so that all signal contributions that are not from the central pixel will cancel out. The noise from all the pixels, however, will add together incoherently with a coefficient that equals the corresponding absolute value of the IFFT components of the ramp filter. The IFFT of the ramp filter represents a "line spread function" of the filtered back projection and has some useful properties for noise estimation. The sum of the absolute values of the points on each side of the zero position approximates well to the centre point value. For a given scan orientation, this means that the noise contribution of all the detector elements except the one that is aligned with the central pixel, approximates well to the noise contribution of the central detector element (neglecting for simplicity the effect of the circular aperture). Because all N pixels along the central detector element have the same coefficient, they will, for the uniform scene, give the same noise contribution for this particular angle (including the central pixel). A conservative estimate of the noise contribution to the signal of all the pixels is therefore $(2N)^{½}$ times the noise contribution of the central pixel for each angular sample. The incoherently added noise for all the M angular positions is similar, resulting in a total noise figure of $(2N \times M)^{½}$ times the noise of the central pixel for one angular sample. If P photoelectrons are created in each pixel during each angular scan, and we assume shot noise to be the main contribution, the intrinsic central pixel noise during one sample would be $P^{½}$.

A 2D detector array with the same frame rate would have the potential to accumulate $M \times P$ photoelectrons per pixel, with $(M \times P)^{½}$ pixel noise, giving a signal-to-noise ratio of $(M \times P)^{½}$. The ideal spin scan TOSCA sensor would also accumulate $M \times P$ photoelectrons per pixel, but with a central pixel noise level of $(2N \times M \times P)^{½}$ times, giving a signal-to-noise ratio of $(M \times P/2N)^{½}$. For array sizes between 32 and 128 this represents approximately an order of magnitude worse results than for an ideal 2-dimensional detector array in terms of noise.

3.3 Effect of misalignment and other optomechanical imperfections on the recorded signal

Noise and errors can also arise from optomechanical imperfections of a mechanically scanning system. In [1], a temporal constant offset by one or a few samples in the reticle based conical scan TOSCA configuration transforms the system point spread function into a doughnut shape, creating blurring and double line features in the scene. A sufficiently large offset degrades the image completely. This issue is less severe in the array based conical scan TOSCA configuration, with a star-shaped detector array, where the number of samples per rotation is significantly smaller due to a smaller scan circle, easing the control requirements of the optics rotational speed.

In this spin scan configuration, the effects of timing jitter or offset are different. A simulation of high resolution reconstruction similar to the one used in [2] was implemented, with a nominal 299 angular scan steps. The nominal case reconstruction is shown in Fig. 4(a).

Because the sample positions across the field of view are defined by the geometrical layout, a constant temporal shift will not affect detector positioning along the scan line. Instead, the scan line angle is shifted, such that a constant offset will rotate the entire image without any other deformation. This was not simulated, as the argument is straightforward. In a practical application, the detector array geometry is defined by photolithography which, thanks to the demands of microelectronic manufacturing, tends to be more than accurate enough to neglect geometrical imperfections such as nonparallellism of the detector elements.

A constantly varying shift can appear if the rotational speed is different from that required by the sample rate and number of angular scans per frame. The reconstructed images will then rotate, and also deteriorate. This is shown in Fig. 4(b), where the rotational speed is 10% too high. This is most likely higher than what might be expected in a real system, but highlights the effects. The image looks almost like a multiple exposure, with a rotation, but there is also an additional angular distortion. The multiple exposure effect arise as the angular scan is done with a 360° rotation, and all scans separated by ~180° will be shifted by the same amount. As

#224954 - $15.00 USD Received 15 Oct 2014; revised 24 Nov 2014; accepted 29 Nov 2014; published 18 Dec 2014

this is an angular distortion, the effect is more accentuated for features closer to the edge. Central features will be less deteriorated, but they will be affected by artifacts generated by peripheral features, typically creating a “veil” over the central part of the image.

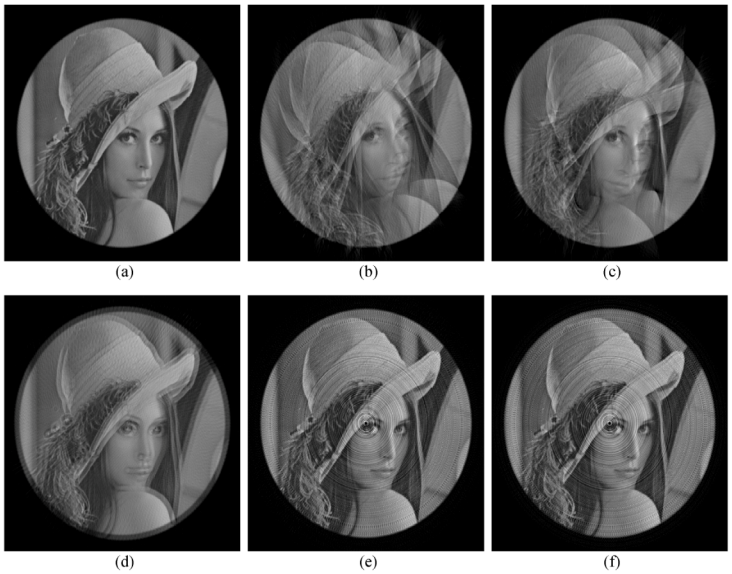

Fig. 4. Simulated high resolution spin scan TOSCA reconstruction to highlight errors related to spin speed errors. (a) Normal reconstruction with 299 angular scans. (b) Reconstruction with a constant, 10% speed error (too high). (c) Reconstruction with a sinusoidally varying phase shift in the scan speed. (d) Reconstruction with the camera misaligned with the rotating optics, orthogonally to the detector orientation. Reconstruction with nonuniform gain (e) and offset (f).

Various other errors are possible in the rotational movement, such as jitter and instability. As an example, the reconstruction in Fig. 4(c) shows a phase shift during the angular scans varying sinusoidally from 0° to 15° and back during one rotation. The resulting features are similar to those of the constant speed variations, with the central “veil” and shape deformation on the sides, but the double exposure effect is only visible in parts of the scene. Also, the scene would not appear to rotate, and small errors of this kind might therefore be slightly more difficult to notice.

Misalignment of the sensor position relative to the rotating optics axis can create severe deformations if the misalignment is in a direction across the detector element orientation, very similar to the constant offset timing deformations seen in the conical scan TOSCA imager [2]. This is illustrated in Fig. 4(d). The deformations observed here, point sources deformed into rings, and lines deformed into double line features are due to the doughnut shaped point spread function. The misalignment that is parallel to the detector orientation, not shown here, is less significant, and creates mainly a circular deformation zone at the edge of the circular scene, similar to the artifacts created in the conical scan TOSCA imager with a misaligned aperture.

The less than 100% fill factor might affect the imaging properties, as point sources passing across the resulting spatially regularly modulated responsivity variations could create unwanted signal modulation. A more generalized modulation could also arise due to spatial inhomogeneity of both detector gain and offset. If temporally stable, this kind of modulation could create circular pattern artifacts, due to the circular detector movement relative to the scene. A simulation of nonuniform gain is shown in Fig. 4(e), and a simulation of nonuniform offset is shown in Fig. 4(f). As can be seen from the reconstructions, the effects of these

#224954 - $15.00 USD Received 15 Oct 2014; revised 24 Nov 2014; accepted 29 Nov 2014; published 18 Dec 2014

nonuniformities have very similar appearances, here exaggerated by using the same random sequence.

4. Experiments

4.1 Experimental setup

A spin scan TOSCA array based imager was built to demonstrate the concept, shown in Fig. 5. The implementation uses three rotating plane mirrors as shown in Fig. 2. The focusing optics, the aperture and the detector array is implemented using a 32 × 32 pixel uncooled PbSe Matrix Core-S focal plane array (FPA) USB camera from New Infrared Technologies with 24 mm focal length, f# = 1.2 germanium optics. By combining signals from columns of pixels, this fast camera can emulate a 32 × 1 array of long detector elements. The uncooled detector chip is specified to have a spectral range from 1.0 to 5.0 μm, with peak responsivity at 3.7 μm. With the germanium optics, the spectral range is reduced to 1.8-5.0 μm.

The camera is not capable of analog binning of a full column; therefore it is running as a 2D focal plane array, with a subsequent software binning. This limits the operation to 100 angular positions per second and limits the photon harvesting efficiency, but enables monitoring of the intrinsic 2D imaging during the angular scans and also eases the camera alignment to the rotating optics. The selective use of pixels inside a 32 pixel diameter circle also enables the emulation of an aperture, which is then unnecessary to implement in hardware. The camera operates in a free-running mode, reporting acquired images when finished.

The rotating optics consists of a rotating mount which holds the three flat mirrors that flip the scene. The unit is connected to a Moog Animatics SmartMotor stepper motor via a timing belt. The angular orientation is slaved to the camera frame rate, with the desired number of angular scan positions per revolution as an input to the control software. Control of the rotating optics and the camera, the signal processing, image reconstruction, live visualization and data storage is implemented in National Instruments' LabView.

Given the limited resolution, simple targets were chosen for the imaging experiments:

1. A mask with a 5 mm diameter circular pinhole, made with a 20 mm diameter circular steel plate mounted on a thick cardboard plate in front of a 300°C blackbody. The TOSCA image was reconstructed from 99 angular scan positions.
2. A mask with two 5 mm pinholes, separated by 30 mm center-to-center in front of a 300°C black body. The reconstruction used 99 angular scan positions.
3. The same setup of two 5 mm pinholes where one pinhole was covered by an uncoated 2 mm thick germanium wafer.
4. "Halloween lantern" cardboard mask shown in Fig. 6, back illuminated by a 300°C black body. Reconstructions were made using a range of angular scan step sizes.
5. Halloween mask, back illuminated by halogen lamp light reflected off white paper. The TOSCA image was reconstructed from 99 angular scan positions.
6. Halloween mask, back illuminated by a 300°C black body, but with the triangular nose of the mask covered by the germanium wafer. The TOSCA image was reconstructed from 99 and 199 angular scan positions, respectively.

#224954 - $15.00 USD Received 15 Oct 2014; revised 24 Nov 2014; accepted 29 Nov 2014; published 18 Dec 2014

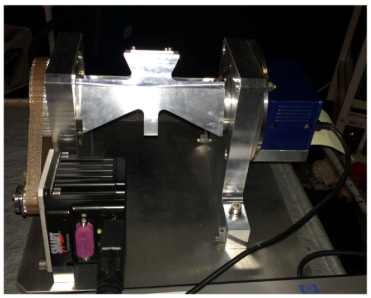

Fig. 5. Experimental spin scan TOSCA camera setup. The main components are the step motor (black, left), the 32 × 32 pixel FPA camera (blue, right), and the rotating optical unit with the three mirrors is in the centre. The optical unit features a counterweight to minimise vibrations.

Fig. 6. Cardboard Halloween mask target used in the experiments.

The germanium substrate approximately halves the transmitted signal from the hot blackbody, reducing the contrast between the mask and the substrate covered apertures by almost an order of magnitude, compared to the contrast between the mask and the blackbody.

The PbSe camera raw images recorded were found to exhibit a non-negligible amount of offset drift. Therefore, a 100 frame temporal average 1-point non-uniformity correction (NUC) was made with a room temperature black body at the beginning of each recording.

4.2 Results

The recording of a 5 mm diameter pinhole back illuminated by a 300°C black body is shown in Fig. 7. Figure 7(a) depicts the raw image from one of the 99 angular scans used to reconstruct a TOSCA image, including the 1-point NUC. In Fig. 7(b), the pixels from the imager that are inside a 32 pixel diameter circle are summed up column by column, creating a 1-dimensional projection of the apertured image. The fact that the background appears as a downward curve stems from the fact that the in-band radiation emanating from the mask through emission and reflection is slightly less than that of the room temperature black body, combined with the fact that the number of pixels summed up on the sides is smaller on the sides than in the middle of the curve. Figure 7(c) shows the effect of the ramp filter on the angular scan in Fig. 7(b). Note the amplification of high-frequency components. Figure 7(d) shows the result of back-projecting the filtered signal onto a matrix. The back projection is here done on a 64 × 64 pixel matrix, using linear interpolation. Figure 7(e) shows the TOSCA reconstruction, the result of summing up all the filtered back projections of the 99 angular scans.

#224954 - $15.00 USD Received 15 Oct 2014; revised 24 Nov 2014; accepted 29 Nov 2014; published 18 Dec 2014

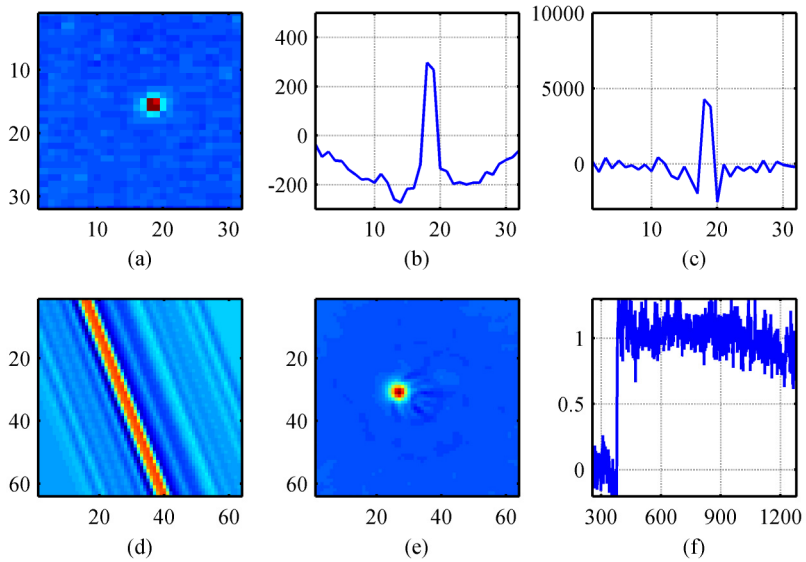

Fig. 7. Recording of a 5 mm diameter pinhole with spin scan TOSCA imager (Media 1). A 300°C black body is behind the pinhole. (a) 32 × 32 pixel FPA snapshot before software binning to the linear format. One such image is used per angular scan step. The scene image is rotated relative to the FPA at each scan. (b) Columnwise sum of FPA pixels inside a 32 pixel diameter aperture. (c) Ramp filtered detector signal. (d) Back projection of the filtered angular scan. (e) TOSCA image reconstructed from 99 filtered back projections. (f) Normalised temporal variation in the total scene (temporal unit: angular scans).

Two noticeable features are the curved fringe patterns and the otherwise relatively smooth background. Finally, Fig. 7(f) shows the total signal from the scene, each point on this curve representing the sum of the curve in Fig. 7(b), indicating the significant temporal detector noise in the FPA. The first part of the curve was made with a room temperature blackbody inserted in the optical path, resulting in a step when it was removed. Figures 7-14 all have a similar structure. The curved fringe pattern in the TOSCA reconstruction appears to be extending from the pinhole-to-center axis. The curvature of the fringes is seen to be stronger closer to the axis of rotation. It could be due to a slight decentering of the focal plane array relative to the rotational axis of the rotational scan. It could, however, also be due to the fact that the pinhole is not entirely centered in the scene.

#224954 - $15.00 USD Received 15 Oct 2014; revised 24 Nov 2014; accepted 29 Nov 2014; published 18 Dec 2014

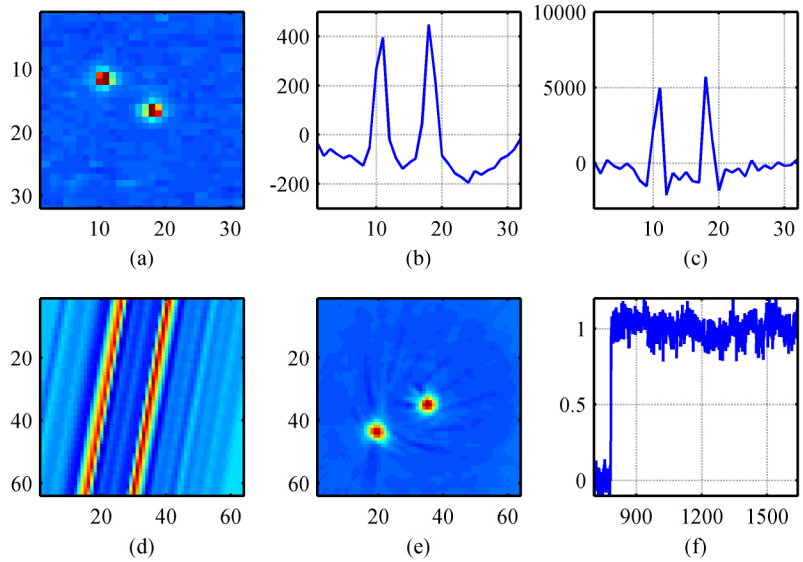

Fig. 8. Double pinhole recording (Media 2). The experiment is similar to that in Fig. 7, but here the target consists of two 5 mm diameter pinholes backlit with a 300°C blackbody. (a) 32 × 32 pixel FPA snapshot. (b) Columnwise sum of FPA pixels inside a 32 pixel diameter aperture. (c) Ramp filtered detector signal. (d) Back projection of the filtered angular scan. (e) TOSCA image reconstructed from 99 filtered back projections. (f) Normalised temporal total scene variation.

Figure 8 shows the TOSCA reconstruction of the double 5 mm diameter pinhole mask, with a 30 mm center-to-center distance. The almost vertical, straight line observed in the reconstruction is due to temporal signal intensity variations in the scene. Again, a curved fringe pattern appears to emanate from the line between the pinholes and the axis between the pinhole and the optical rotational centre.

Figure 9 shows another double pinhole image with properties similar to that of Fig. 8, but here a 2 mm uncoated germanium window is reducing the contrast with the mask by a factor ~8. Even though the fringe pattern arising from the dominant pinhole, similar to the one in Fig. 7 is significant, it is easy to discern the second, dimmer pinhole.

Figure 10 shows the reconstruction of the Halloween mask, backlit by the 300°C blackbody. The signal is significantly above the noise level of the detector array, as seen by the temporal signal in Fig. 10(f). A circular fringe pattern can be observed in the reconstruction in Fig. 10(e), especially at the forehead, and between the nose and the eyes. This pattern is consistent with the gain/offset patterns seen in Figs. 4(e)-4(f), and suggests that the 1-point NUC made is not sufficient, and that a 2-point NUC is necessary. The pixellation of the triangular shape of the eyes have all but vanished. Structural mouth details are visible.

#224954 - $15.00 USD Received 15 Oct 2014; revised 24 Nov 2014; accepted 29 Nov 2014; published 18 Dec 2014

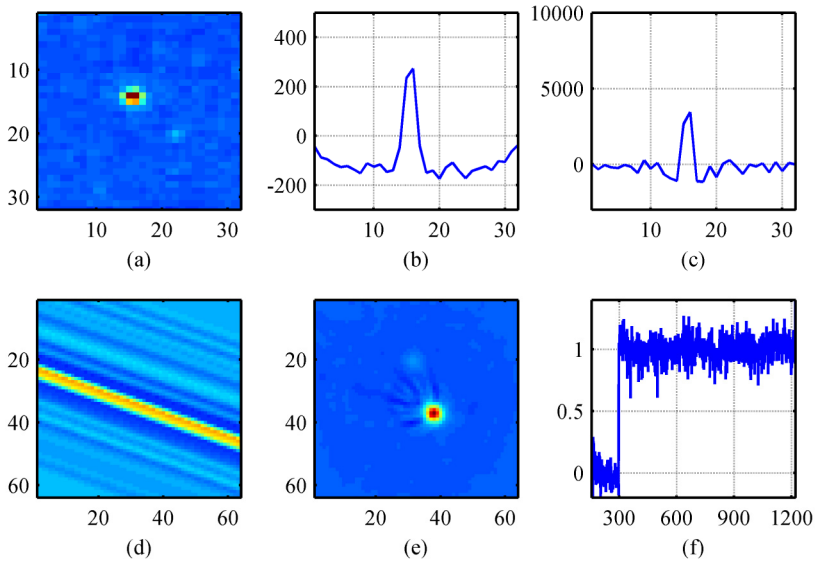

Fig. 9. Double pinhole recording, similar to that in Fig. 8, but with one pinhole covered with an uncoated germanium substrate (Media 3). (a) 32 × 32 pixel FPA snapshot. (b) Columnwise sum of FPA pixels inside a 32 pixel diameter aperture. (c) Ramp filtered detector signal. (d) Back projection of the filtered angular scan. (e) TOSCA image reconstructed from 99 filtered back projections. (f) Normalised temporal variation in the scene.

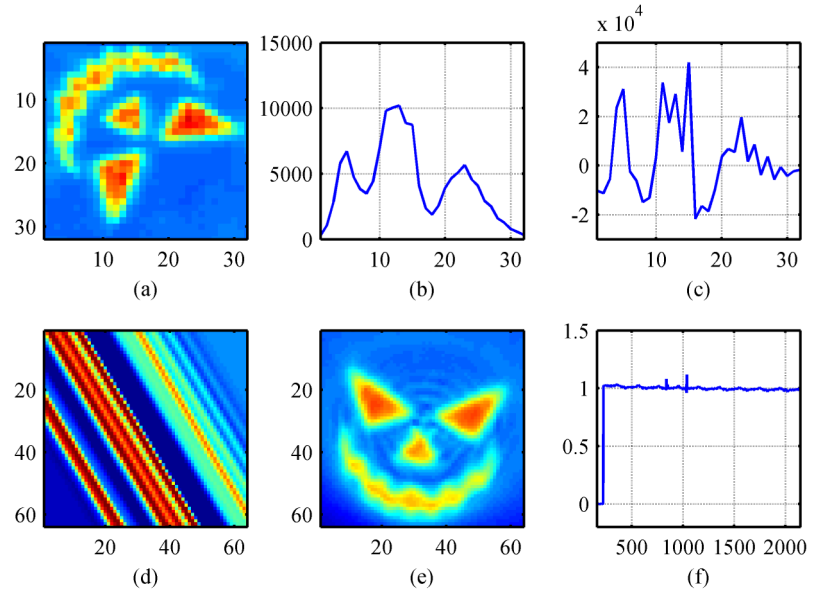

Fig. 10. Recording of Halloween mask backlit by a 300°C blackbody (Media 4). (a) 32 × 32 pixel FPA snapshot. (b) Columnwise sum of FPA pixels inside a 32 pixel diameter aperture. (c) Ramp filtered detector signal. (d) Back projection of the filtered angular scan. (e) TOSCA image reconstructed from 99 filtered back projections. (f) Normalised temporal total scene variation. The video associated to Figs. 10-14 shows the effect of scene dynamics (rotation).

The Halloween mask reconstruction in Fig. 11 is similar to that of Fig. 10, but with a halogen lamp illuminated copying paper replacing the blackbody backlighting. The signal is much weaker, the (contrast) signal-to-noise level of the FPA frames being only 3-5. This is an order of magnitude lower than in Fig. 10. A similar fringe pattern is also visible, but weaker.

#224954 - $15.00 USD Received 15 Oct 2014; revised 24 Nov 2014; accepted 29 Nov 2014; published 18 Dec 2014

The pixellation of the eyes have again essentially vanished and the mouth structure is recognizable, but the fringe pattern has deteriorated parts of the image, particularly the nose sides. Figure 11(f) shows temporal intensity drift, which may account for part of the deterioration.

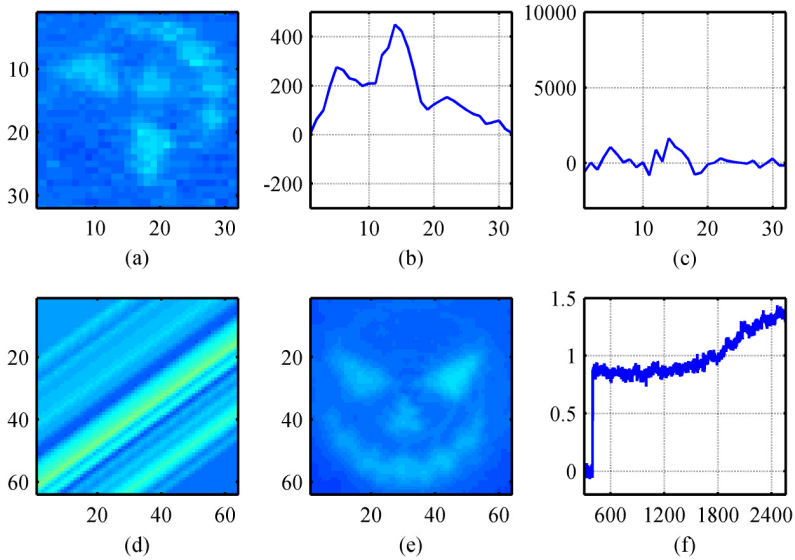

Fig. 11. Recoding of Halloween mask target backlit by halogen lamp illuminated copying paper (Media 5). (a) 32 × 32 pixel FPA snapshot. (b) Columnwise sum of FPA pixels inside a 32 pixel diameter aperture. (c) Ramp filtered detector signal. (d) Back projection of the filtered angular scan. (e) TOSCA image reconstructed from 99 filtered back projections. (f) Normalised temporal total scene variation.

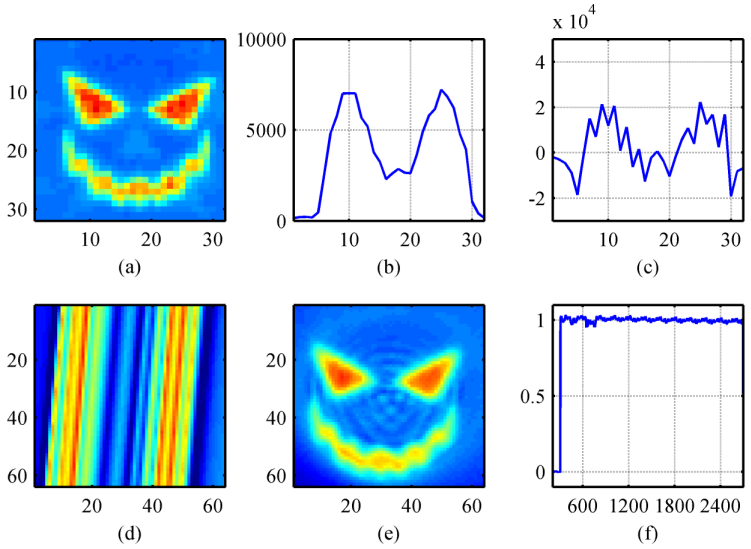

Fig. 12. Recording of Halloween mask target backlit by a 300°C blackbody as in Fig. 10, but with an uncoated germanium substrate covering the nose (Media 6). (a) 32 × 32 pixel FPA snapshot. (b) Columnwise sum of FPA pixels inside a 32 pixel diameter aperture. (c) Ramp filtered detector signal. (d) Back projection of the filtered angular scan. (e) TOSCA image reconstructed from 99 filtered back projections. (f) Normalised temporal variation in the total scene.

#224954 - $15.00 USD Received 15 Oct 2014; revised 24 Nov 2014; accepted 29 Nov 2014; published 18 Dec 2014

In Fig. 12, the Halloween mask is imaged as in Fig. 9, but with a 2 mm thick uncoated germanium substrate covering the nose of the mask. Two fringe patterns are clearly visible, a circular fringe pattern, and a centrally located approximately triangular interference pattern. The nose section is barely visible in the raw FPA image. Due to the strong interference, the nose is indistinguishable from the fringe pattern in the reconstructed image. With the strong signal the total intensity, shown in Fig. 12(f), shows relatively limited relative variations in the scene intensity integrated over the synthetic circular aperture.

To verify that the fringe pattern is not due to insufficient angular resolution, the experiment in Fig. 12 was repeated, but with more than twice the number of angular steps, from 99 in the previous experiment to 199. The result is shown in Fig. 13. As can be seen in Fig. 13(e), the image is virtually identical to Fig. 12(e), the nose still blurred by the fringe pattern. This shows that the 99 angular scans are not limiting the system imaging properties.

In order to check if the interference pattern could be due to the low number of elements used in the imaging, the 32 × 32 pixel array was shifted slightly to simulate a 64 linear array by using two frames with an approximate 180° shift to generate an interleaved pattern, as described in section 2.2. The result is shown in Fig. 14. This time the processing was not done live, but post-processed, as the original system software did not have the interleaving algorithm implemented. The setup did not use an exact 180° shift, as 199 angular scans were used to generate the first series of 32 pixel measurements, corresponding to a complete rotation, and 199 angular scans, shifted by 100 samples, were used to generate the second series of measurements. This represents a systematic angular error for the interleaved samples of ½ angular step, or less than 1°. For the central (software binned) detector, this corresponds to a maximum sideways error of ¼ detector pixel unit at the edge. In comparison, the 64 elements synthesized detector pattern has a ½ detector pixel unit separation.

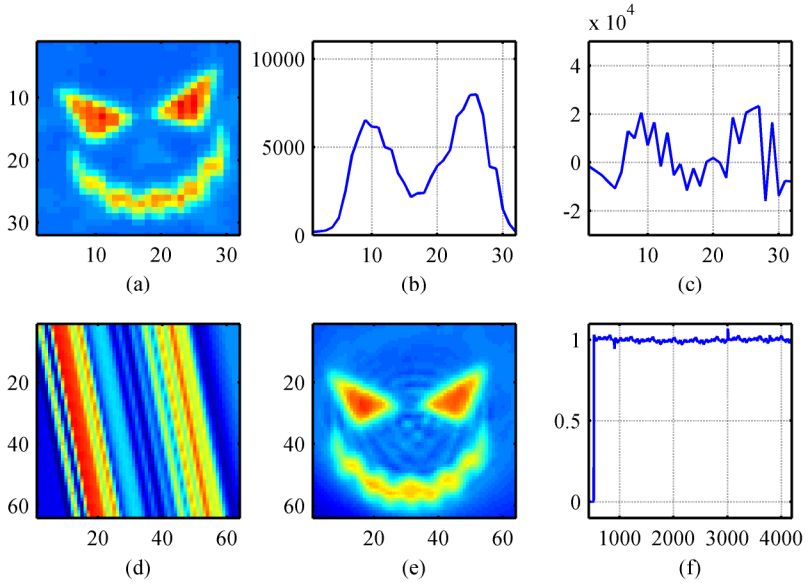

Fig. 13. Recording of Halloween mask with a germanium nose as in Fig. 11, but now using 199 angular scans (Media 7). (a) 32 × 32 pixel FPA snapshot. (b) Columnwise sum of FPA pixels inside a 32 pixel diameter aperture. (c) Ramp filtered detector signal. (d) Back projection of the filtered angular scan. (e) TOSCA image reconstructed from 99 filtered back projections. (f) Normalised temporal variation in the total scene.

As seen in Fig. 14(a), the stitching of the ~180° images leads to jaggedness due to misalignment. The jaggedness is enhanced by the ramp filter due to its high frequency nature, as seen in Figs. 14(b) and 14(c). The reconstruction in Fig. 14(d) has significant thin circular

#224954 - $15.00 USD Received 15 Oct 2014; revised 24 Nov 2014; accepted 29 Nov 2014; published 18 Dec 2014

ring artifacts and, to a lesser degree, Moiré patterns. Specifically, the more pronounced ring pattern as compared to previous reconstructions suggests that there is a considerable low-frequency component in the nonuniformity. A slowly varying responsivity across the array will appear in the processing as alternating high and low values in the interlaced detector element responses.

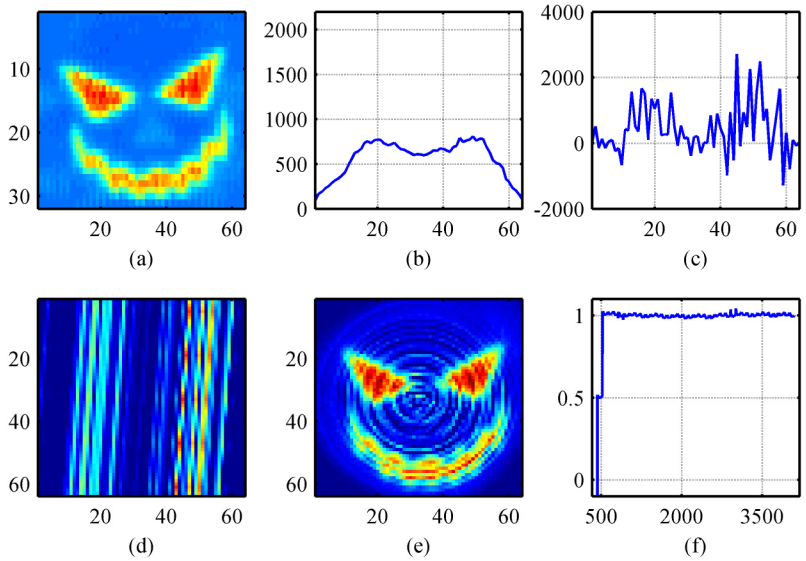

Fig. 14. Recording of Halloween mask with a germanium nose as in Fig. 12, but using two sets of 199 angular scans, shifted by 99 FPA frames (Media 8). (a) 32 × 64 pixel fusion of two interleaved 32 × 32 pixel FPA frames, separated by a ~180° field of view rotation. (b) Columnwise sum of FPA pixels inside a 32 by 64 pixel diameter elliptic aperture. (c) Ramp filtered detector signal. (d) Back projection of the filtered angular scan. (e) TOSCA image reconstructed from two 199 filtered back projections, separated by 100 angular scans. (f) Normalised temporal variation in the total scene. The behaviour is peculiar in the beginning due to the 100 sample shift.

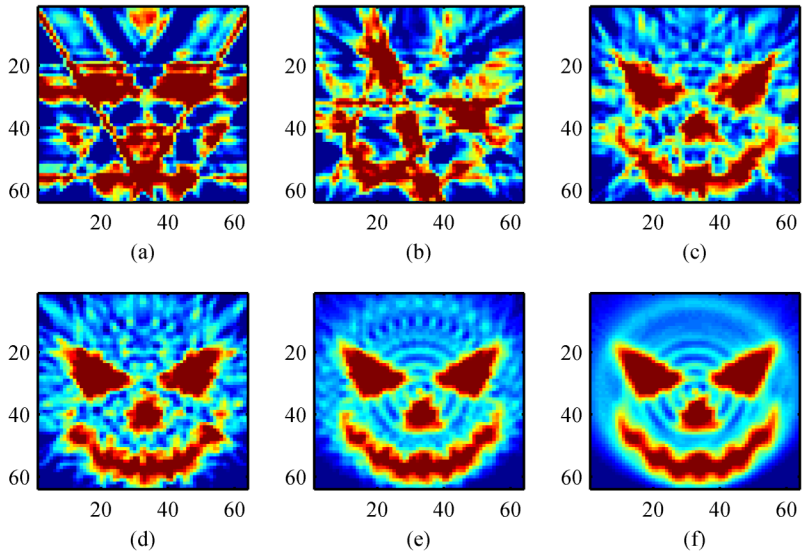

Fig. 15. TOSCA reconstructions of Halloween mask with 32 elements and a varying number of angular scans: (a) 3 scans, (b) 5 scans, (c) 9 scans, (d) 11 scans, (e) 33 scans and (f) 99 scans.

#224954 - $15.00 USD Received 15 Oct 2014; revised 24 Nov 2014; accepted 29 Nov 2014; published 18 Dec 2014

Kak and Slaney [4] have indicated that the number of samples per scan and the number of angular scan steps should be approximately equal to give a well-balanced image. A test was made to see the difference as the number of scans was increased. This is shown in Fig. 15, with 3, 5, 9, 11, 33 and 99 scans, respectively. As can be seen, with 3 scans, it is extremely difficult to recognize even very crude aspects of the mask. With 5 scans, it is possible to recognize the mask if given an image. The general outline of the major components becomes visible with around 10 scans, and fine structures become recognizable with 33 scans, approximately equal to the number of detector elements. At 99 scans, the jagged angular aspects of the artifacts have disappeared, at around π times the detector count. This corresponds to the aperture perimeter, measured in detector element width units.

5. Discussion

The new spin scan TOSCA imager has demonstrated clear imaging properties, despite the low number of detector elements used in this implementation. An issue with so few elements is that even with a high number of angular scan steps, significant interference fringe patterns will occur, also close to the objects in the scene. One advantage is that the outline of the objects can be relatively accurately represented with a sufficient number of angular steps. With few samples and angular steps for a given desired end resolution, the artifacts will inevitably be of a higher importance than in the case of a high detector count and a large number of angular scans, limiting faithful reproduction of features in images with high dynamics. Complexity also affects this capability. In the reconstructions in Figs. 7-9, the artifacts are relatively easy to separate from the scene features, even with order of magnitude variation in contrast. With the more complex scenarios seen in Fig. 10 onwards, however, the artifacts accumulate, deteriorating low contrast features beyond recognition. The main frequency component of the artifact ripples had frequency values close to the Nyquist limit of the detector array density. Increasing the number of angular steps in this scenario proved to not add significant enhancements, as, at 99, the number of steps was already ~π times the number of the 32 detector elements across the field of view. This showed that the main reason for the artifacts was the limited number of detector elements.

It was initially assumed that shifting the detector array sideways ¼ pixel would enable a doubling of the resolution and hence reduce the artifacts somewhat. However, in the experiment with this implementation several hurdles were encountered that actually degraded the image compared to the results achieved without the stitching. One hurdle was the difficulty with doing sub-element alignment, creating jaggedness in the sensor image, and the other was the detector nonuniformity.

The circular artifacts highlight the need for good sensor uniformity. In this demonstrator, a 2-point NUC could have reduced the magnitude of the artifacts, but in a linear detector array configuration, inhomogeneities within each detector cannot be taken away directly using a simple 2-point NUC. In principle, vignetting could also affect system nonuniformity, but if the vignetting effect is circularly symmetrical to the field of view, it can easily be compensated for after the reconstruction. Some inhomogeneities could also stem from stray light entering the camera, partly because the scan mechanism was made out of reflective materials. Evidence of this is difficult to assess in the still images, but some are visible in the videos, in particular the videos depicting the pinhole masks. Another less problematic issue was the synthetic aperture used, which had a different resolution in the two directions. This would represent less of a problem here, however, as the Halloween mask is homogeneous outside the facial features. Another issue that was not tested here is that the interleaving structure presented at the end would be particularly vulnerable to temporally changing scenes.

6. Conclusion

This paper presents the first spin scan tomographic scanning (TOSCA) imager, together with several optical scanning solutions. An uncooled imager operating in the 1.8-5.0 μm mid-

#224954 - $15.00 USD Received 15 Oct 2014; revised 24 Nov 2014; accepted 29 Nov 2014; published 18 Dec 2014

infrared spectral range was demonstrated. The system here used a camera structure with a resistor network readout electronics limiting the readout to 100 angular scans per second, but a dedicated sensor architecture should be able to operate at least one to two orders of magnitude faster. With 32 line detectors and 99 angular steps, the system was able to image simple scenes with contrast dynamics of about one order of magnitude. In very complex scenes, though, this was proven to be insufficient due to artifacts accumulating. The artifacts observed were mainly due to a limited number of detector lines, combined with nonuniform detector responsivity.

An attempt was made to double the imaging resolution by using a ¼ pixel detector offset, combined with 180° detector shift, interleaving the resulting signals. Several hurdles were making this particular implementation less successful. Allthough images were produced, the resulting quality was degraded, mainly due to errors provoked by the interleaved fusion of the two images, rotated relative to each other.

Detailed physics-based simulations were used to identify the effect of error sources such as misalignment, temporal sampling errors and scan speed variations. The analysis identified the need for a precise angular reference, but initial simulations indicated that it might not be necessary to have detailed angular position readout for each sample, provided rotational inertia is significant. Simulations and experiments also highlighted the sensitivity to nonuniform detector responsivity. The corrections to the nonuniformities are not trivial and hence put requirements on detector quality. The proposed configuration has some limitations in pure imaging with high contrast due to a low number of angular scan orientations creating characteristic curved or circular line artefacts, but is sufficient if objects of interest are located on an otherwise homogeneous background. Measurements using the experimental setup verified performance predicted through theory and simulations.

Acknowledgments

The author is grateful to Prof Svein Erik Hamran and Dr Torbjørn Skauli for helpful discussions and able guidance, and to Mr Pål Halvorsen for doing the SolidWorks implementation of the camera design.

#224954 - $15.00 USD Received 15 Oct 2014; revised 24 Nov 2014; accepted 29 Nov 2014; published 18 Dec 2014